ARTICLES

Probabilistic assessment of sea level during the last interglacial stage

Robert E. Kopp[1,2], Frederik J. Simons[1], Jerry X. Mitrovica[3], Adam C. Maloof[1] & Michael Oppenheimer[1,2]

With polar temperatures ~3–5 °C warmer than today, the last interglacial stage (~125 kyr ago) serves as a partial analogue for 1–2 °C global warming scenarios. Geological records from several sites indicate that local sea levels during the last interglacial were higher than today, but because local sea levels differ from global sea level, accurately reconstructing past global sea level requires an integrated analysis of globally distributed data sets. Here we present an extensive compilation of local sea level indicators and a statistical approach for estimating global sea level, local sea levels, ice sheet volumes and their associated uncertainties. We find a 95% probability that global sea level peaked at least 6.6 m higher than today during the last interglacial; it is likely (67% probability) to have exceeded 8.0 m but is unlikely (33% probability) to have exceeded 9.4 m. When global sea level was close to its current level (≥ -10 m), the millennial average rate of global sea level rise is very likely to have exceeded 5.6 m kyr^{-1} but is unlikely to have exceeded 9.2 m kyr^{-1}. Our analysis extends previous last interglacial sea level studies by integrating literature observations within a probabilistic framework that accounts for the physics of sea level change. The results highlight the long-term vulnerability of ice sheets to even relatively low levels of sustained global warming.

As a result of industrial activity, greenhouse gas concentrations now exceed levels reached on Earth at any time within the past 800 kyr (ref. 1). Given a climate sensitivity of 2–4.5 °C per doubling of carbon dioxide levels[2], current greenhouse gas concentrations—without considering any further increases—are sufficient to cause an equilibrium warming of 1.4–3.2 °C. Among the many effects expected to accompany this warming is a rise in global sea level (GSL)[2], which is defined as the mean value of local sea level (LSL) taken across the ocean. This rise is driven primarily by thermal expansion of sea water and by melting land ice. Uncertainties in ice sheet behaviour make it difficult to predict sea level rise using prognostic models, but by the end of the twenty-first century, GSL could exceed today's value by more than one metre (refs 3, 4). As changes of this magnitude have no precedent in recorded history, to understand them and to compile observations against which to test models of future climate change, it is necessary to turn to the geological record.

In this Article, we analyse a new compilation of geographically dispersed sea level indicators spanning the last interglacial stage (LIG), which climaxed about 125,000 years ago (125 kyr ago). The LIG (also known as the Eemian stage, its local northern European name, and as Marine Isotope Stage 5e) is of special interest for three reasons: (1) it is recent enough that it is possible to obtain some sea level records with high temporal resolution and many more observations with lower temporal resolution; (2) due in large part to enhanced Northern Hemisphere insolation, global and polar temperatures may have been slightly warmer than at present; and (3) several lines of evidence suggest that GSL was higher than today, perhaps by 4–6 m (ref. 1), and that the Greenland Ice Sheet and possibly also the West Antarctic Ice Sheet[5,31] were significantly smaller than they are now.

During the LIG, greenhouse gas concentrations were comparable to pre-industrial Holocene levels[7], but Earth's orbital eccentricity was more than twice the modern value[8]. Energy balance modelling predicts that, as a consequence, summer temperatures between 132 and 124 kyr ago on all land masses except Antarctica were at least 0.5 °C warmer than today[9], while a more complete climate model indicates summer temperatures 2–4 °C warmer than today in most of the Arctic[6]. Ice core data from both Greenland and Antarctica suggest polar temperatures in both hemispheres of about 3–5 °C warmer than today[1], comparable to the 3–6 °C of Arctic warming that is expected to accompany 1–2 °C of global warming[10]. In Europe, pollen data suggest middle Eemian summer temperatures about 2 °C warmer than present[11]. While the change in global mean temperature is uncertain, sea surface temperatures in the equatorial Pacific[12] and Atlantic[13] were about 2 °C warmer than pre-industrial levels.

Synthesizing geological sea level indicators into a global reconstruction requires accounting for regional variability. Differences between LSL and GSL arise because—contrary to an analogy commonly taught in introductory classes—adding water from melting land ice to the ocean is not like pouring water into a bathtub. Many factors other than the changing volume of water in the ocean modulate the influence of melting ice sheets on LSL. These factors include: the direct gravitational effect of the distribution of ice, water and sediment on the sea surface (or geoid), solid Earth deformation and its associated gravitational signature, perturbations to both the magnitude and orientation of the Earth's rotation vector, and time-varying shoreline geometry[14–16], as well as changes in ocean and atmosphere dynamics[17]. In addition, LSLs are influenced by tectonic uplift and thermal subsidence.

As a consequence of these factors, LSLs at Pacific islands far from the late Pleistocene ice sheets were 1–3 m higher in the middle Holocene than today, even though GSL was essentially unchanged[18]. Similarly, even if GSL was never higher than today, LSLs several metres higher than present could have occurred far from the former Laurentide Ice Sheet (for example, in Australia) early in the LIG, and comparably high LSLs could have occurred closer to the former ice sheet (for example, in the Caribbean) late in the LIG[19]. Without accurate and precise dating of the relevant sea level indicators and an appreciation of the difference between LSL and GSL, such patterns could

[1]Department of Geosciences, [2]Woodrow Wilson School of Public and International Affairs, Princeton University, Princeton, New Jersey 08544, USA. [3]Department of Earth and Planetary Sciences, Harvard University, Cambridge, Massachusetts 02138, USA.

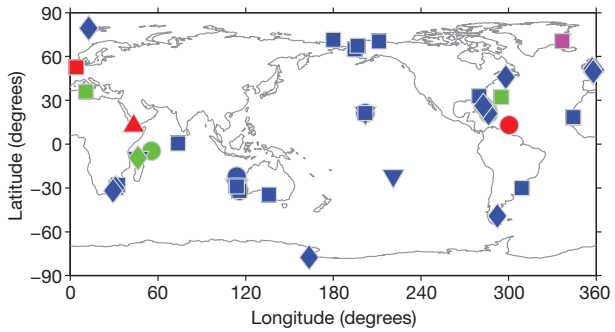

Figure 1 | Sites with at least one sea level observation in our database. The symbol shapes reflect the nature of the indicators (upward triangles, isotopic; circles, reef terraces; downward triangles, coral biofacies; squares, sedimentary facies and non-coral biofacies; diamonds, erosional). The colours reflect the number of observations at a site (blue, 1; green, 2; magenta, 3; red, 4 or more).

produce the false appearance of a magnified or diminished GSL highstand. In order to estimate ice sheet history from sea level records, it is thus necessary to account for physical factors like gravitation and solid Earth deformation. Conversely, because these effects cause LSL changes to differ with distance from an ice sheet, a global database of LSL indicators can potentially address not just whether global ice volume was smaller during the LIG than today, but also what combination of melting ice sheets, if any, was responsible for higher GSL.

We construct a database of sea level indicators that is as comprehensive as possible (Figs 1, 2; full data set available in Supplementary Information) and use it to estimate the posterior probability distribution of LSL as a function of space and time and of GSL and ice sheet volumes as functions of time. We must cope with variable geochronological uncertainty, as well as with variable errors in sea levels inferred from proxy data and in estimates of regional long-term tectonic uplift or thermal subsidence. In addition, some of the data provide only upper or lower bounds to sea level. Where possible, we also want to take advantage of quasi-continuous sequences, in which relative timing is known with greater precision than absolute dates. These sequences include a stacked global oxygen isotope curve from benthic foraminifera[20], as well as series of LSL measurements inferred from sedimentary facies in the Netherlands[21] and from hydrological modelling of foraminiferal oxygen isotopes in the Red Sea[22]. (These series are described in detail in Supplementary Information.)

Statistical approach

The ultimate goal of our analysis is to determine the posterior probability distribution of LIG sea level and ice volume through time, conditioned upon the measurements in our database. Inherent in the method is the assumption that both the prior and posterior distributions are multivariate Gaussian.

We construct a prior probability distribution from the global oxygen isotope curve and its associated age model[20], as described in detail in Methods and Supplementary Information. To do this, we use a physical model of LSL that calculates the eustatic, gravitational, deformational and rotational effects of melting ice sheets[15,16,23]. We estimate the mean and covariance of the prior distribution by averaging the values and covariances of the LSLs and of GSL obtained by running many alternative ice sheet histories through a forward physical model. These histories themselves are sampled from two underlying distributions: a distribution for global ice volume over time based upon ref. 20 and a distribution for individual ice sheet volumes conditioned upon global ice volume. This latter distribution is based upon random perturbations of a model of Last Glacial Maximum (LGM)-to-present ice sheet volume[24] with additional allowances made for ice sheets smaller than their present volumes. To approximate thermosteric effects resulting

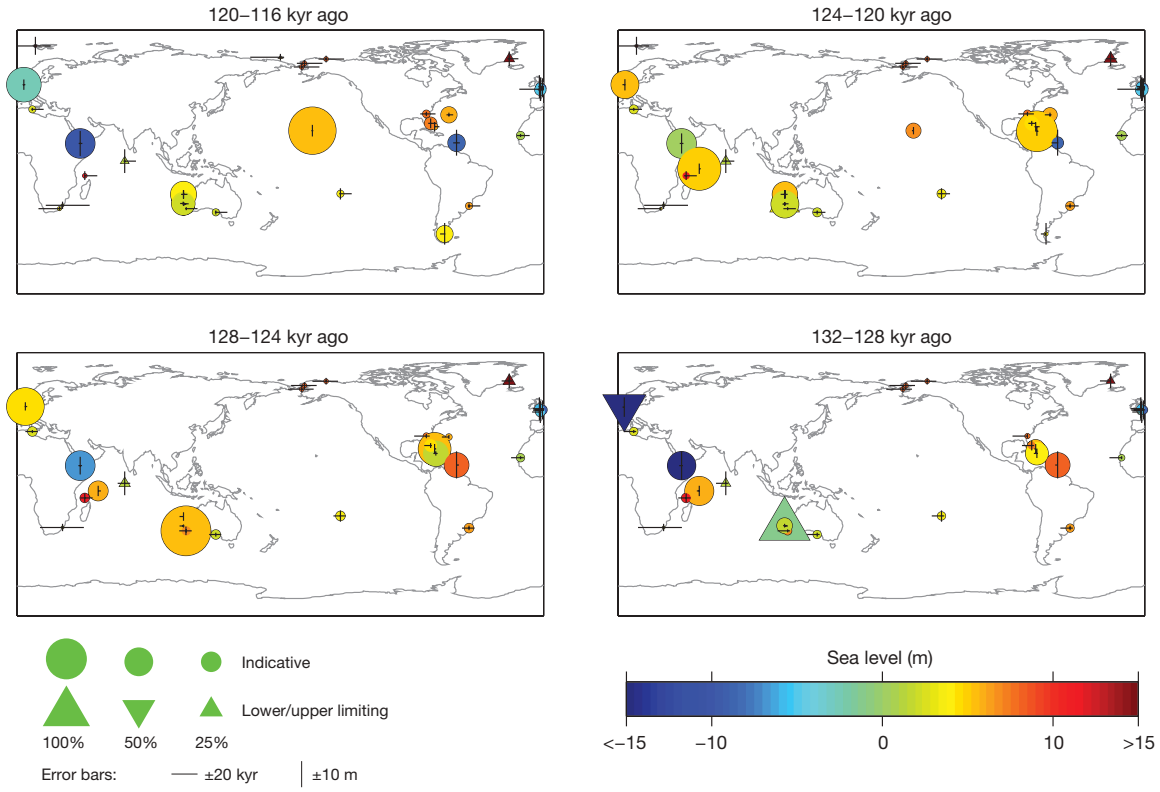

Figure 2 | Localities at which LSL data exist in our database, for time slices through the LIG. The diameter of each circle scales as indicated with the probability that the corresponding data point occurs in the indicated interval. The horizontal (vertical) lines are proportional to the standard deviations of the age (sea level) measurements. The intersection of the lines reflects the mean age estimate relative to the age window; a rightward skew reflects a mean estimate earlier than the middle of the window. Data that provide only upper or lower sea level bounds are indicated by downward and upward triangles, respectively. Colours indicate the mean sea level estimate in metres above present value. Some symbols overlap; for a complete table of observations, see Supplementary Information.

from changes in mean ocean temperature and salinity, we add two Gaussian terms: a term independent of time and GSL with a mean of 0 m and a standard deviation of 2 m, and a term that varies with global ice volume (-1.6 ± 0.6 m per 100 m equivalent sea level (e.s.l.) ice sheet growth). The temporal covariance of these thermosteric terms has an e-folding time of 2 kyr. The uncertainty within the thermosteric terms is large enough to also accommodate small contributions from other sources, such as small mountain glaciers present today but not included in the LGM-to-present ice model.

To construct the posterior distribution of sea level at any arbitrary point in space and time, we start with the simpler problem of estimating the posterior probability distribution of sea level at the points included in our database and then interpolate to calculate values at points not in our database. We employ a three-step Gibbs sampler[25] to sample the Bayesian network illustrated in Fig. 3.

In the first step, we calculate corrected measurements of LSLs (**s**) by adjusting the altitude of our proxy observations (**z**) for their depositional settings (**D**), which account for the relationship between proxy altitudes and sea level elevation at the time of formation, and for the background regional uplift or subsidence. The former correction incorporates sedimentological and geomorphological knowledge, such as the fact that most coral observations in the database are of species that grow between 0 and 5 m below mean low tide level[26,27], as well as information about local tidal range. The latter correction is based upon an estimate of the regional uplift or subsidence rate (**u**) and a sample from the posterior distribution of measurement ages (**g**). In selecting or constructing uplift or subsidence rate estimates, we have avoided estimates from the literature that assume LIG sea level as a reference point.

In the second step, we employ Gaussian process regression to estimate the true sea levels (**f**). Gaussian process regression[28], of which the commonly used geospatial technique of kriging interpolation is a well-known example, treats a field (such as sea level) as a collection of random variables drawn from a multivariate Gaussian distribution. By specifying the covariance structure of the field, knowledge about the relevant physics affecting the process can be incorporated into the modelling without constraining it to fit a particular forward model.

In the third step, we use the Metropolis-Hastings algorithm[29] to draw a new Markov chain Monte Carlo sample of the ages (**g**), based upon the measured ages (**t**) and the current estimate of the true sea levels (**f**). Repeating this sequence many times allows us to sample the posterior probability distribution for LSL and GSL in a way that satisfies the measurements to within their uncertainties.

Equipped with an estimate of the posterior probability distribution, we can then answer questions such as 'what was the maximum GSL attained during the LIG' and 'what was the fastest rate at which GSL rose when it was within 10 m of its present value?' (As discussed below, we focus on rates above the -10 m threshold because the Laurentide Ice Sheet was comparable in size to the modern Greenland Ice Sheet by the time GSL rose to this level in the Holocene.) To answer such questions, we draw many samples from the posterior distribution and examine the distribution of answers based on these samples. We report these answers as exceedance values. For instance, the 95% probability exceedance value of GSL is exceeded in 95% of all samples. If the 95% exceedance value is 6.6 m, we can reject the hypothesis that sea level never exceeded 6.6 m at the 95% confidence level. Note that the answer to such questions is not identical to the answer one would get by looking at the median projection of GSL and reading its maximum; the maximum of the median would be the 50% probability exceedance value if all time points were perfectly correlated, but such is not the case. The median reconstruction instead represents the best estimate for GSL at each specific point in time, whereas the exceedance values are calculated across the entire LIG interval.

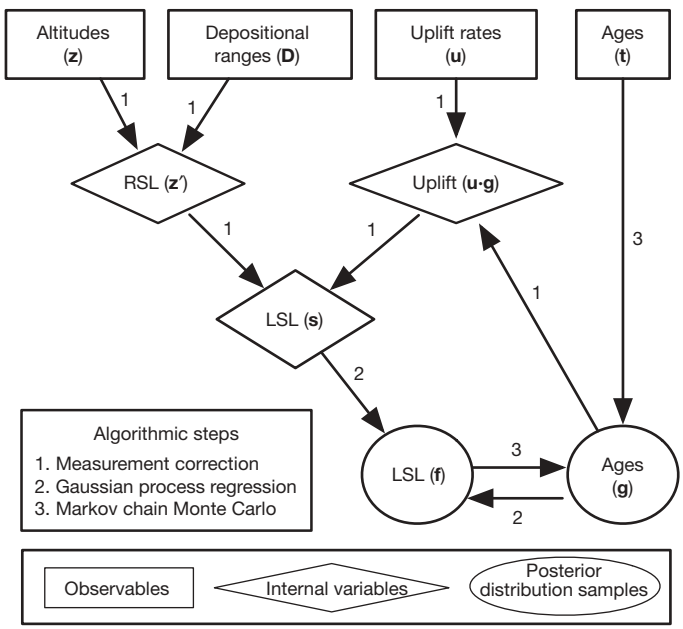

Figure 3 | Schematic illustration of the process used in our statistical analysis. See text for details.

Results of global analysis

Applying our algorithm to the full data set of LIG sea level indicators yields a GSL curve (Fig. 4a) with a median projection that peaks at 124 kyr ago at 7.2 ± 1.3 m (67% confidence interval). Further analysis reveals a 95% probability of having exceeded 6.6 m at some time during the LIG highstand and a 67% probability of having exceeded 8.0 m (Fig. 5, solid line). It is unlikely (33% probability) that GSL exceeded 9.4 m.

To test the sensitivity of these results, we analysed seven subsets of the data: one subset excluding the Red Sea oxygen isotope curve, and six either excluding or including only (1) coral data, (2) erosional features, or (3) facies interpretations (Supplementary Information).

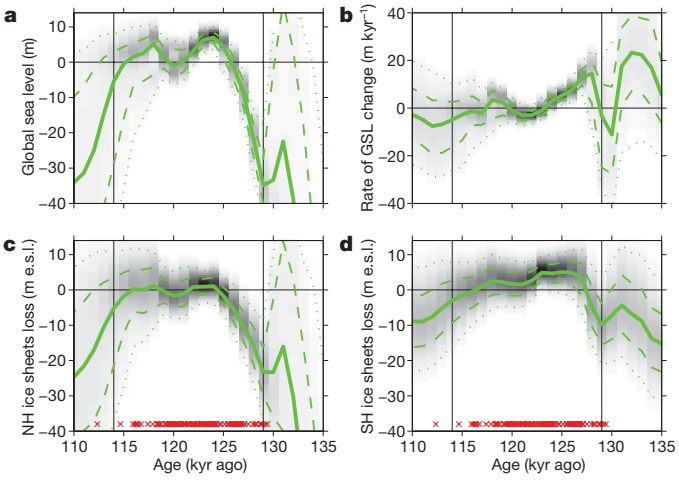

Figure 4 | Probability density plots of GSL and ice volume during the LIG. **a**, Global sea level (GSL); **b**, 1,000-year average GSL rates; **c**, Northern Hemisphere (NH) ice volume; and **d**, Southern Hemisphere (SH) ice volume. Heavy lines mark median projections, dashed lines the 16th and 84th percentiles, and dotted lines the 2.5th and 97.5th percentiles. Red crosses mark median posterior estimates of sample ages. Vertical lines mark the interval when >30% of samples from the distribution have standard deviations of GSL <30% of the prior standard deviation (and are thus included in calculations of exceedance probabilities). The horizontal line at 0 indicates modern values in **a**, **c** and **d** and unchanging GSL in **b**. We urge caution in interpreting ice volume projections (**c**, **d**) owing to the use of a Gaussian distribution to represent a non-Gaussian prior. e.s.l., equivalent sea level.

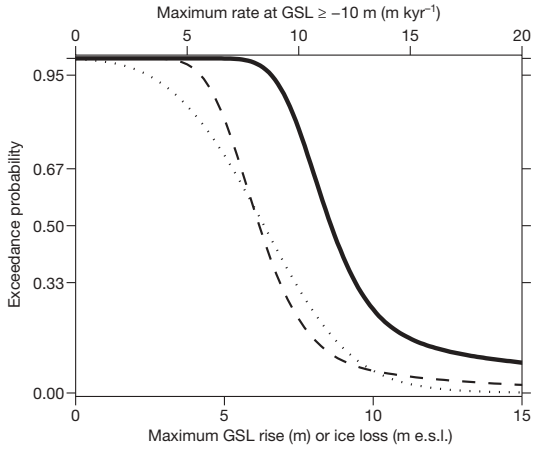

Figure 5 | Exceedance values calculated from the posterior probability distribution. The solid line shows GSL rise, the dashed line shows the 1,000-year average rate of change of GSL when GSL is at or above −10 m, and the dotted line shows ice loss in the hemisphere with the least ice loss.

The results from these subsets were fairly consistent. Across all subsets, the median projection peaked between 6.4 and 8.7 m. With the exception of the subset containing only erosional features, the 95% probability exceedance value ranged from 5.7 to 7.0 m, the 67% probability value ranged from 7.3 to 8.7 m, and the 33% probability value ranged from 8.4 to 10.5 m. (The values for the subset containing only erosional features were slightly lower and more broadly spread, with 95%, 67% and 33% values of −0.3 m, 3.9 m and 6.8 m, respectively. The spread reflects the relatively high uncertainty on this projection, which results in large part from a smaller data set.) We therefore consider our results to be reasonably robust with respect to different observations.

The 95%, 67% and 33% probability exceedance values for 1,000-year average GSL rise rate during the interval when GSL was ≥−10 m are 5.6 m kyr^{-1}, 7.4 m kyr^{-1} and 9.2 m kyr^{-1}, respectively (Fig. 4b; Fig. 5, dashed line). We emphasize that these values by no means exclude faster intervals of sea level rise lasting for less than one millennium.

We can also attempt to answer questions about the magnitude of ice sheet volume based on the posterior probability distribution, but we must do so with caution. The distribution of Northern Hemisphere ice volume, in particular, can only be roughly approximated with a Gaussian, as it has a hard upper bound set by the fact that there is only about 7 m e.s.l. of Northern Hemisphere ice available to melt today. Because of this limitation, although we directly present the hemispheric ice volume posteriors in Fig. 4c, d, we make only one fairly conservative inference regarding ice sheet volumes. The posterior distribution suggests a 95% probability that both Northern Hemisphere ice sheets and Southern Hemisphere ice sheets reached minima at which they were at least 2.5 m e.s.l. smaller than today, although not necessarily at the same point in time (Fig. 5, dotted line). We can make no strong statements about in which hemisphere the ice shrunk to a greater extent; in 59% of samples, it was the Southern Hemisphere and in 41% of samples, it was the Northern Hemisphere. Additional sea level proxies close to the ice sheets would help increase the precision of these estimates, as might a non-Gaussian model for the prior distribution.

Comparison to previous estimates

Previous estimates of LIG sea level, which were generally in the range 4–6 m, were based on interpretations of LSL at a small number of localities. The Fourth Assessment Report of the IPCC[1] highlighted Hawaii and Bermuda[30]; other authors[31] also include observations from the Bahamas, Western Australia and the Seychelles Islands. All these localities are relatively tectonically stable and experience only slow thermal subsidence, associated with the cooling of the lithosphere. If one had to draw conclusions about GSL from a small number of LSL measurements, these are reasonable sites at which to look.

Other commonly considered localities, such as Barbados[32] and the Huon Peninsula[33], are rapidly uplifting localities. These sites have advantages as relative sea level recorders, most notably that terraces recording sea levels below present are readily accessible. Assuming these sites have experienced a steady rate of uplift, they can help uncover sea level variations over fairly short timescales. However, they are poor sites from which to draw conclusions about absolute sea levels, as recovering this information requires a precise estimate of uplift rate. Because our method incorporates knowledge about the associated uncertainties, we can include both stable and uplifting sites into our analysis.

To our knowledge, only one previous study[19], which used a fairly limited set of observations, has attempted to account for the effects of glacial isostatic adjustment in drawing conclusions about GSL and ice volume from LIG sea level records. As that study demonstrated, understanding the influence of these effects is critical, as otherwise LSL highstands could easily be falsely interpreted as reflecting global highstands. Our statistical model uses the covariance between local and GSL, derived from many runs of a forward physical model, to account for the gravitational, deformational and rotational effects of the ice–ocean mass redistribution. Our results indicate that the apparent high GSL during the LIG is indeed real, though previously underestimated.

Rates of sea level change

Our results suggest that during the interval of the LIG when sea level was above −10 m, the rate of sea level rise, averaged over 1 kyr, was very likely to have reached values of at least about 5.6 m kyr^{-1} but was unlikely to have exceeded 9.2 m kyr^{-1}. Our data do not permit us to resolve confidently rates of sea level change over shorter periods of time. Our inferences are consistent with estimates of the rate of the contribution of Laurentide Ice Sheet meltwater to GSL during the early Holocene; the Laurentide Ice Sheet contribution is estimated to account for about 7 m kyr^{-1} during the period when GSL climbed above −10 m (ref. 34).

Ice volume during the late deglacial rise at the start of the LIG was only slightly larger than at present. The Laurentide Ice Sheet would have been a shrunken remnant of its once extensive mass—or, perhaps two small remnants, one over Québec and Labrador and one over eastern Nunavut and Baffin Island, as in the early Holocene[34,35]. As the Laurentide Ice Sheet was within a factor of two in size of the present Greenland Ice Sheet, its dynamics may have been analogous to those of the Greenland Ice Sheet. The results from the LIG suggest that, given a sufficient forcing, the present ice sheets could sustain a rate of GSL rise of about 56–92 cm per century for several centuries, with these rates potentially spiking to higher values for shorter periods.

Discussion

Although it is the approach most commonly taken when the LIG is used as an analogue for near-future warming, GSL and global ice volume cannot be accurately inferred by a qualitative examination of LSL at a handful of localities. Better control is afforded by a more thorough approach that combines, as we do, an extensive database of sea level indicators with a probabilistic assessment of their interpretive and geochronological errors. The results of our analysis support the common hypothesis that LIG GSL was above the current value, but contrary to previous estimates, we conclude that peak GSL was very likely to have exceeded 6.6 m and was likely to have been above 8.0 m, though it is unlikely to have exceeded 9.4 m.

The LIG was only slightly warmer than present, with polar temperatures similar to those expected under a low-end, ~2 °C warming scenario. Nonetheless, it appears to have been associated with substantially smaller ice sheets than exist at present. Achieving GSL in excess of 6.6 m higher than present is likely to have required major melting of both the Greenland and the West Antarctic ice sheets, an

inference supported by our finding that both Northern and Southern hemisphere ice volumes are very likely to have shrunk by at least 2.5 m e.s.l. relative to today. Incorporating a large database of palaeoclimatic constraints thus highlights the vulnerability of ice sheets to even relatively low levels of sustained global warming.

METHODS SUMMARY

We assembled our database, which includes observations from 42 localities, through an extensive literature search for indicators with best estimates of ages between 140 and 90 kyr ago. To each indicator we assigned a depth range of formation or deposition based upon geomorphological and sedimentological interpretation. See Methods and Supplementary Information for full details of the database, the statistical analysis algorithm, and the physical model used to generate the covariance function.

Full Methods and any associated references are available in the online version of the paper at www.nature.com/nature.

Received 27 February; accepted 11 November 2009.

1. Jansen, E. *et al.* in *Climate Change 2007: The Physical Science Basis* (eds Solomon, S. *et al.*) 433–498 (Cambridge Univ. Press, 2007).
2. Meehl, G. A. *et al.* in *Climate Change 2007: The Physical Science Basis* (eds Solomon, S. *et al.*) 747–845 (Cambridge Univ. Press, 2007).
3. Rahmstorf, S. A semi-empirical approach to projecting future sea-level rise. *Science* **315,** 368–370 (2007).
4. Grinsted, A., Moore, J. C. & Jevrejeva, S. Reconstructing sea level from paleo and projected temperatures 200 to 2100 AD. *Clim. Dyn.* doi:10.1007/s00382-008-0507-2 (published online 6 January 2009).
5. Cuffey, K. M. & Marshall, S. J. Substantial contribution to sea-level rise during the last interglacial from the Greenland ice sheet. *Nature* **404,** 591–594 (2000).
6. Otto-Bliesner, B., Marshall, S., Overpeck, J., Miller, G. & Hu, A. Simulating Arctic climate warmth and icefield retreat in the Last Interglaciation. *Science* **311,** 1751–1753 (2006).
7. Petit, J. *et al.* Climate and atmospheric history of the past 420,000 years from the Vostok ice core, Antarctica. *Nature* **399,** 429–436 (1999).
8. Berger, A. & Loutre, M. F. Insolation values for the climate of the last 10 million years. *Quat. Sci. Rev.* **10,** 297–317 (1991).
9. Crowley, T. & Kim, K. Milankovitch forcing of the Last Interglacial sea level. *Science* **265,** 1566–1568 (1994).
10. Katsov, V. M. *et al.* in *Arctic Climate Impact Assessment* (eds Symon, C., Arris, L. & Heal, B.) Ch. 4, 99–150 (Cambridge Univ. Press, 2004).
11. Kaspar, F., Kühl, N., Cubasch, U. & Litt, T. A model-data comparison of European temperatures in the Eemian interglacial. *Geophys. Res. Lett.* **32,** L11703, doi:10.1029/2005GL022456 (2005).
12. Lea, D. The 100,000-yr cycle in tropical SST, greenhouse forcing, and climate sensitivity. *J. Clim.* **17,** 2170–2179 (2004).
13. Weldeab, S., Lea, D., Schneider, R. & Andersen, N. 155,000 years of West African monsoon and ocean thermal evolution. *Science* **316,** 1303–1307 (2007).
14. Farrell, W. E. & Clark, J. A. On postglacial sea level. *Geophys. J. R. Astron. Soc.* **46,** 647–667 (1976).
15. Mitrovica, J. X. & Milne, G. A. On post-glacial sea level: I. General theory. *Geophys. J. Int.* **154,** 253–267 (2003).
16. Kendall, R., Mitrovica, J. & Milne, G. On post-glacial sea level – II. Numerical formulation and comparative results on spherically symmetric models. *Geophys. J. Int.* **161,** 679–706 (2005).
17. Yin, J., Schlesinger, M. E. & Stouffer, R. J. Model projections of rapid sea-level rise on the northeast coast of the United States. *Nature Geosci.* **2,** 262–266 (2009).
18. Mitrovica, J. X. & Milne, G. A. On the origin of late Holocene sea-level highstands within equatorial ocean basins. *Quat. Sci. Rev.* **21,** 2179–2190 (2002).
19. Lambeck, K. & Nakada, M. Constraints on the age and duration of the last interglacial period and on sea-level variations. *Nature* **357,** 125–128 (1992).
20. Lisiecki, L. E. & Raymo, M. E. A. Pliocene-Pleistocene stack of 57 globally distributed benthic δ^{18}O records. *Paleoceanography* **20,** 1–17 (2005).
21. Zagwijn, W. H. Sea-level changes in the Netherlands during the Eemian. *Geol. Mijnb.* **62,** 437–450 (1983).
22. Rohling, E. J. *et al.* High rates of sea-level rise during the last interglacial period. *Nature Geosci.* **1,** 38–42 (2008).
23. Mitrovica, J., Wahr, J., Matsuyama, I. & Paulson, A. The rotational stability of an ice-age earth. *Geophys. J. Int.* **161,** 491–506 (2005).
24. Peltier, W. R. Global glacial isostasy and the surface of the ice-age Earth: the ICE-5G (VM2) model and GRACE. *Annu. Rev. Earth Planet. Sci.* **32,** 111–149 (2004).
25. Banerjee, S., Carlin, B. P. & Gelfand, A. E. *Hierarchical Modeling and Analysis for Spatial Data* (Chapman & Hall/CRC, 2003).
26. Lighty, R. G., Macintyre, I. G. & Stuckenrath, R. *Acropora palmata* reef framework: a reliable indicator of sea level in the western Atlantic for the past 10,000 years. *Coral Reefs* **1,** 125–130 (1982).
27. Camoin, G. F., Ebren, P., Eisenhauer, A., Bard, E. & Faure, G. A 300,000-yr coral reef record of sea level changes, Mururoa atoll (Tuamotu archipelago, French Polynesia). *Palaeogeogr. Palaeoclimatol. Palaeoecol.* **175,** 325–341 (2001).
28. Rasmussen, C. & Williams, C. *Gaussian Processes for Machine Learning* (MIT Press, 2006).
29. Hastings, W. K. Monte Carlo sampling methods using Markov chains and their applications. *Biometrika* **57,** 97–109 (1970).
30. Muhs, D. R., Simmons, K. R. & Steinke, B. Timing and warmth of the Last Interglacial period: new U-series evidence from Hawaii and Bermuda and a new fossil compilation for North America. *Quat. Sci. Rev.* **21,** 1355–1383 (2002).
31. Overpeck, J. T. *et al.* Paleoclimatic evidence for future ice-sheet instability and rapid sea-level rise. *Science* **311,** 1747–1750 (2006).
32. Schellmann, G. & Radtke, U. A revised morpho- and chronostratigraphy of the Late and Middle Pleistocene coral reef terraces on Southern Barbados (West Indies). *Earth Sci. Rev.* **64,** 157–187 (2004).
33. Esat, T. M., McCulloch, M. T., Chappell, J., Pillans, B. & Omura, A. Rapid fluctuations in sea level recorded at Huon Peninsula during the penultimate glaciation. *Science* **283,** 197–202 (1999).
34. Carlson, A. E. *et al.* Rapid early Holocene deglaciation of the Laurentide ice sheet. *Nature Geosci.* **1,** 620–624 (2008).
35. Tamisiea, M. E., Mitrovica, J. X. & Davis, J. L. GRACE gravity data constrain ancient ice geometries and continental dynamics over Laurentia. *Science* **316,** 881–883 (2007).

Supplementary Information is linked to the online version of the paper at www.nature.com/nature.

Acknowledgements We thank J. R. Stroud, L. D. Brown and B. McShane for statistical guidance, and M. Bender, B. Horton, D. Nychka and D. Peltier for comments. We also thank G. Spada for providing his SELEN sea level code, which we used for preliminary calculations incorporated in a previous version of the statistical model. Computing resources were substantially provided by the TIGRESS high performance computer centre at Princeton University, which is jointly supported by the Princeton Institute for Computational Science and Engineering and the Princeton University Office of Information Technology. R.E.K. was supported by a postdoctoral fellowship in the programme on Science, Technology, and Environmental Policy at the Woodrow Wilson School of Princeton University.

Author Contributions R.E.K. compiled the database, developed the statistical analysis method, and co-wrote the paper. F.J.S. contributed to the development of the statistical analysis method and co-wrote the paper. J.X.M. developed the physical sea level model and co-wrote the paper. A.C.M. contributed to the compilation of the database and co-wrote the paper. M.O. supervised the project and co-wrote the paper.

Author Information Reprints and permissions information is available at www.nature.com/reprints. The authors declare no competing financial interests. Correspondence and requests for materials should be addressed to R.E.K. (rkopp@alumni.caltech.edu).

METHODS

Database of LIG sea level indicators. We characterize each LIG sea level indicator (indexed by i) by five parameters: its geographical position ($\mathbf{r}_i$), its measured altitude with respect to mean tide level (z_i), its measured age (t_i), the range of depths at which it might have formed ($\mathbf{D}_i$), and the estimated local uplift or subsidence rate (u_i). Some of the observations are censored, in that they provide only an upper or lower bound to sea level. When more than one observation comes from the same locality, we also record stratigraphic order and, where available, estimates of the relative ages of observations. With the exception of geographical position, each of these variables has uncertainties that we assume follow a Gaussian distribution. For some values, including all depositional depth ranges, uniform distributions between two limits a and b may be a better choice than Gaussian ones. In these cases, we substitute a Gaussian distribution with the same mean and standard deviation as the uniform distribution, that is, $(b-a)/\sqrt{12}$. Depositional ranges $\mathbf{D}_i$ are thus replaced with Gaussian estimates d_i. The full database is supplied in Supplementary Information.

Prior distribution. We assume that sea level is a Gaussian process with a spatially and temporally varying covariance described by the function $k(\mathbf{r}_i, g_i; \mathbf{r}_j, g_j)$. There is no uncertainty on spatial location $\mathbf{r}_i$, but the temporal variable is g_i, the model age (see Fig. 3). We approximate k by $\hat{k}$, which is produced by sampling alternative histories from a forward model that incorporates the relevant physics. To stabilize the estimate and reduce variability related to finite sample size, we smooth $\hat{k}$ with a Gaussian temporal taper function: $\hat{k}(\mathbf{r}_i, g_i\,;\, \mathbf{r}_j, g_j) = \hat{k}_0(\mathbf{r}_i, g_i;\, \mathbf{r}_j, g_j)\exp\left[-(g_i-g_j)^2/\tau^2\right]$, as discussed in the Supplementary Information. To produce the results described in the main text, we employed $\tau = 3$ kyr. Results from other values are shown in Supplementary Information.

The prior probability distribution is based upon the age model of ref. 20, which places the start of the deglaciation at about 135 kyr ago and the start of the LIG highstand at about 127 kyr ago. For consistency, we have aligned the Red Sea and Dutch sequences against this record and excluded from the main analysis three observations from the Houtman-Abrohlos Islands[36,37] whose ages are inconsistent with this model. There is, however, considerable disagreement among current age models. Reference 38 (adopted in ref. 22) places the start of the highstand at about 125 kyr ago, 2 kyr later than ref. 20, while ref. 39 places the start of the deglaciation at between 137 and 142 kyr ago, 2–7 kyr earlier. Our results do not attempt to address these differences, and should be viewed in the context of the ref. 20 timescale.

Physical model. The physical model is based on a gravitationally self-consistent sea-level equation[15] that extends earlier work[14] to take exact account of shoreline migration due to either local sea-level changes (which give rise to offlap or onlap) and changes in the extent of grounded, marine-based ice. The calculations are performed using a pseudo-spectral sea-level solver[16,40] with a truncation at spherical harmonic degree and order 256. The solver incorporates the feedback on sea level of contemporaneous, load-induced perturbations in the Earth's rotation vector[16], where these perturbations are computed using the new ice-age rotation theory of ref. 23. The sensitivity to Earth structure is embedded within viscoelastic surface load and tidal Love numbers[41,42]. We adopt spherically symmetric, self-gravitating, Maxwell viscoelastic Earth models. The elastic and density structure of these models is given by the seismic model PREM (ref. 43). The viscosity profile is discretized into three layers, including: (1) an extremely high (essentially elastic) lithospheric lid of thickness LT; (2) a uniform viscosity from the base of the lithosphere to 670 km depth (that is, the sub-lithospheric upper mantle) which we denote as ν_{UM}; and (3) a uniform lower mantle viscosity (that is, from 670 km depth to the core-mantle boundary) denoted by ν_{LM}. We consider a suite of 72 such Earth models generated by using the following choices: LT = 70, 95, or 120 km; $\nu_{\mathrm{UM}} = 0.3$, 0.5, 0.8 or 1.0×10^{21} Pa s; $\nu_{\mathrm{LM}} = 2$, 3, 5, 8, 10, or 20×10^{21} Pa s.

As described in Supplementary Information, we generate an estimate of the prior sea level covariance $\hat{k}$ by running the model 250 times with different ice sheet histories and randomly selected viscosity profiles. From these runs, we compute the covariance among LSLs at evenly spaced points, GSLs and ice sheet volumes, as well as at the exact coordinates of the sites in our database, and we store the results as a lookup table. Total ice volume in the different ice sheet histories is sampled from a distribution based upon the ref. 20 global oxygen isotope curve. The ice volume of individual ice sheets is sampled from a probability distribution for individual ice sheet volumes that is conditional upon total global ice volume. This latter distribution is constructed from random perturbations of LGM-to-present ice models[24].

36. Eisenhauer, A., Zhu, Z., Collins, L., Wyrwoll, K. & Eichstätter, R. The Last Interglacial sea level change: new evidence from the Abrolhos islands, West Australia. *Int. J. Earth Sci.* **85,** 606–614 (1996).
37. Zhu, Z. R. *et al.* High-precision U-series dating of Last Interglacial events by mass spectrometry: Houtman Abrolhos Islands, western Australia. *Earth Planet. Sci. Lett.* **118,** 281–293 (1993).
38. Thompson, W. G. & Goldstein, S. L. Open-system coral ages reveal persistent suborbital sea-level cycles. *Science* **308,** 401–405 (2005).
39. Thomas, A. L. *et al.* Penultimate deglacial sea-level timing from uranium/thorium dating of Tahitian corals. *Science* **324,** 1186–1189 (2009).
40. Mitrovica, J. X. & Peltier, W. R. On postglacial geoid subsidence over the equatorial ocean. *J. Geophys. Res.* **96,** 20053–20071 (1991).
41. Peltier, W. R. The impulse response of a Maxwell Earth. *Rev. Geophys. Space Phys.* **12,** 649–669 (1974).
42. Wu, P. *The Response of a Maxwell Earth to Applied Surface Mass Loads: Glacial Isostatic Adjustment.* M.Sc. thesis, Univ. Toronto (1978).
43. Dziewonski, A. & Anderson, D. Preliminary reference Earth model. *Phys. Earth Planet. Inter.* **25,** 297–356 (1981).